CHARACTERIZATION OF THE COMPRESSIVE AND FRACTURE BEHAVIOR, AS WELL AS THE RESIDUAL TENSILE STRENGTH OF A POLYURETHANE FOAM

By

YANLI ZHANG

Bachelor of Science

Mechanical Engineering Technology

Oklahoma State University

Stillwater, the United States

2004

Submitted to the Faculty of the
Graduate College of the
Oklahoma State University
in partial fulfillment of
the requirements for
the Degree of
MASTER OF SCIENCE
May, 2007

CHARACTERIZATION OF THE COMPRESSIVE AND FRACTURE BEHAVIOR, AS WELL AS THE RESIDUAL TENSILE STRENGTH OF A POLYURETHANE FOAM

Thesis Approved:

Dr. Hongbing Lu

Thesis Adviser

Dr. C.E. Price

Dr. Demir Coker

Dr. A. Gordon Emslie

Dean of the Graduate College

ACKNOWLEGEMENTS

First, I would like to express my appreciation to Dr. Hongbing Lu for his instruction on the research. I will always cherish Dr. Lu's attitude toward teaching and research. I would like to thank Dr. Lu for his generous financial support and for the opportunity to let me work in the Polymer Mechanics Lab. Also I would like to thank Dr. C. E. Price and Dr. D. Coker for serving on my committee, and I appreciate Dr. Price's teaching on corrosion engineering and Dr. Coker's guidance on fracture mechanics.

Secondly, I would like to thank American Bureau of Shipping for sponsoring this research project with Dr. Wang as technical contact. I acknowledge Dr. Wang for his valuable feedback on the results. I also thank Dr. Huiyang Luo for his technical instruction on the experiments, and thank Dr. Huang Gang for helping me understand the theory of viscoelasticity.

Furthermore, I would like to thank Mr. Gitogo Churu, Mr. Nitin Daphalapurkar and Mr. Jitandra Bambharoliya for the help they provided during the time we worked in the same lab. Also I would like to thank the School of Mechanical and Aerospace Engineering at OSU for giving me the opportunity to pursue my masters degree.

Finally, I would like to thank my father Wenlu Zhang and my mother Shubiao Gao for the priceless love they have shown for me and excellent example they set for my life. Also, My husband, Hong Gao, has always been very supportive during the process to pursue this degree. At Last I want to mention my two children, Huacheng and Justin. The joy from you inspired me to work harder and let me understand further the meaning of life.

TABLE OF CONTENTS

LIST OF TABLES

LIST OF FIGURES

Figure Page

CHAPTER I

INTRODUCTION

1.1 **Background**

Cellular solids were widely applied in different fields in recent years because of their unique features. They often have high specific strength and high specific energy absorption rate. Foam is a subclass of cellular solids. Polymeric foam has been widely used in marine, automotive, aerospace and other industries as a core material for the sandwich structures. The material used in this study is a rigid polyurethane foam that served as the external internal insulation material for large Liquefied Natural Gas (LNG) tanks. There are about 5% chopped fibers embedded in polyurethane foam. Fibers are generally oriented randomly in parallel planes. Perpendicular to the planes is the weak direction, along which the properties are lower. The foam is under mechanical loads due to the weight of the LNG, as well as the impact force generated through sloshing of the LNG. To use the foam properly for insulation in LNG tanks, it is imperative to understand the mechanical behavior of the foam under loading conditions experienced by the foam at service temperatures. LNG is stored at ~ ─ 170 °C. The foam close to the liner of LNG tank will be at this temperature, while the outer layer foam will be at a temperature close to room temperature. To investigate the durability of the foam for use as thermal insulation for a LNG tank, this study will investigate the compressive response

at these two temperatures. Since cracks are often observed in the foam, fracture tests were conducted to determine the stress intensity factor to ensure that the applied stress intensity factor does not exceed the fracture toughness.

The foam is subjected to repetitive compression induced by frequent LNG sloshing and the repetitive loading will cause cumulative damage in the material. When the amplitude of the compressive stress is low, it takes a large number of cycles of compressive loading to cause significant damage. But if the amplitude of the compressive stress is high, a few cycles can cause severe damage. Once damage occurs in the foam, the residual tensile strength will deteriorate, and needs to be quantified for design analysis.

1.2 Literature Review

Polymeric foam has found increasing applications in aerospace, marine, automotive industry and other fields in recent years due to its light weight and high specific energy adsorption capability (Landro et al., 2001; Weiser et al., 2000). Gibson and Ashby (1997) summarized extensively the research results on foam material in various applications. They explained the complex behavior of the foam material and investigated the correlation between foam microstructure and its properties. The properties of foam depend strongly on the cellular structures, such as the cell size and shape, and density. Closed-cell foam is more complicated than open-cell foam because the gas or fluid trapped inside the cell during compression will affect the material properties. Foam material often demonstrates strain rate dependent behavior because of the viscoelastic nature of the parent material. Many researchers have characterized the compressive

behavior of different polymeric foams under quasi-static and dynamic loading condition (Saha et al., 2005; Subhash et al., 2006). Saha et al. (2005) and Subhash et al. (2006) investigated the effect of density, microstructure and strain rate on the compression behavior of polymeric foams and found that the peak stress and energy absorption depend strongly on the stain rate, density, microstructure and the type of foam material. Song et al. (2005) investigated the strain rate effects on the elastic and early cell-collapse responses of a polyurethane foam, and found that both then collapse strength and Young's modulus are rate dependent. Kyriakides et al. (1995) have studied the effect of strain rate on the compressive strength of unidirectional ASS/PEEK composite. They found that increasing the strain rate will increase the compressive strength. Papka and Kyriakides (1998) studied the compressive response and crushing behavior of rate dependent polycarbonate honeycomb under displacement controlled quasi-static loading. They found that the response is characterized by a sharp rise to maximum load followed by a drop down to an extended plateau which is terminated by a sharp rise in load. The foam has the same deformation characteristics as the honeycomb. Recently, the foam research has extended to nanoscale. Luo and Lu and Leventis (2006) investigated the compressive behavior of isocyanate-crosslinked silica aerogel, considered to be a nanofoam, at high strain rates. The results showed that Young's modulus and collapse strength have strong dependence on the strain rate.

To better understand the relation between microstructure and bulk properties. Many researchers relies on numerical simulation to find the mechanisms on the deformation behavior of the foam. But simulating the foam response is a well known computational

challenge because of the complexity of the foam microstructure. Brydon et al. (2005) simulated the densification of open-cell foam microstructure. They were able to get a good correlation between the microstructure and bulk properties at lower to medium strain rates. But, for foam with higher relative density at higher deformation rates, cells are partially and fully closed, simulating the response poses a challenge. The gas and fluid trapped inside the cell also complicate the material response. Liu et al. (2005) Studied the crushability of open-cell structural polymeric foams. They created a model to correlate the density and the crushability for certain polymeric foam. It makes it easier to choose a certain type of material for a specific application. On the fracture behavior of the foams, Avci et al. (2004), Kabir et al. (2006) and Choi et al. (2003) investigated the Mode-I fracture toughness for several polymer foams and polymer composites.

1.3 Scope of this work

In this study, the mechanical behavior of rigid polyurethane foam was investigated. Compression tests at five different strain rates, 10^{-3}, 10^{-2}, 10^{-1}, 1, 10, s^{-1}, Mode-I fracture test and residual tensile strength test were carried out to characterize the properties of the foam. The strain rates and temperature used in experiment are similar to those used in service. Compression tests were performed at five different strain rates: 10^{-3}, 10^{-2}, 10^{-1}, 1, 10, s^{-1}, under quasi-static loading condition for both in-plane and out-of-plane. Characterization was made at two temperatures: room temperature and – 170 °C. The relationship between Young's modulus and strain rate, between collapse strength and strain rate were fitted into equations. The relaxation master curve was constructed from the compression data obtained at different strain rates and compressive relaxation results

at different temperatures. The effects of strain rate and temperature on the properties were investigated. Fracture tests were conducted to determine Mode-I fracture toughness. Repetitive tensile strength at 1.5% compressive stain after six different compression cycles: 0, 10, 25, 50, 75, 100, was measured.

CHAPTER II

STRAIN RATE AND TEMPERATURE EFFECT ON THE COMPRESSIVE RESPONSE OF THE FOAM

2.1 Material

The material used in this study is fiber glass reinforced polyurethane foam. The foam material was supplied by GTT through arrangement with ABS. Its glass transition temperature is 165 °C as measured by Dynamic Mechanical Analysis (DMA) and its density is 0.13 g/cm^3. Figure 2.1 shows the microtomography of the foam and we can see it is an open-cell foam. The foam was machined into samples of different sizes and shapes to satisfy the experimental requirements for compression, tension and fracture. The ϕ0.7"x0.5" (ϕ indicates diameter) cylindrical sample is used for compressive tests at stain rate range 10^{-3}/s ~10^{1}/s, ϕ3.0"x1.0" is used to study the temperature effect, while ϕ3.0"x3.0" cylindrical sample is used for relaxation tests. The reason to use ϕ3.0"x1.0" sample for investigation of the effect of temperature is because these tests need to be conducted at relative high strain rates, which require a thinner sample at the maximum velocity the MTS can reach. The duration of each test needs to be as short as possible at low temperature so that the sample temperature remains low during the test. The single-edge-notch bending (SENB) sample with details given in Chapter IV, is used to measure the fracture toughness of the material according to ASTM D5045-99 standard. The dog-

bone shaped sample with details shown in Chapter V, revised from tensile sample described in ASTM D1623-03 for rigid cellular plastics, is used to measure the residual tensile strength after repetitive compression. The samples for compression test were prepared in the Polymer Mechanics Laboratory at Oklahoma State University. All ϕ0.7"x0.5" compressive foam samples were cut using 7/8" hole saw. The ϕ3.0"x3.0" and ϕ3.0"x1.0" samples were machined by JZ systems using water-jet cutting. All samples were polished with a sand paper after machining to generate smooth surface for testing. Except for those to determine the effect of temperature, the experiments were performed at room temperature at (23±1°C) and relative humidity 55±5%. The compressive tests were conducted at room temperature and cryogenic temperature (~ –170 °C). For tests at about –170 ºC, the foam samples were immersed in the liquid nitrogen overnight to reach thermal equilibrium before they were tested.

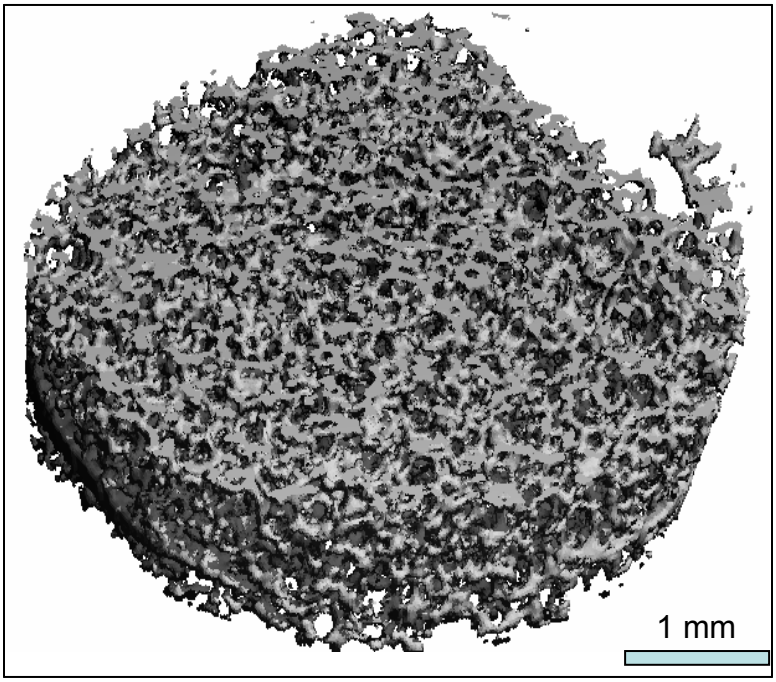

Figure 2.1 Microtomography of polyurethane foam

2.2 Quasi-static experiment set up

An MTS servo-hydraulic test system, with Instron digital controller and data acquisition system, was used for testing at quasi-static state. Load-displacement data were recorded simultaneously as a function of time. A 5 KN load cell was used for ϕ0.7"x0.5" samples, while a 247 KN load cell was used for the ϕ3.0"x3.0" and ϕ3.0"x1.0" samples. Figure 2.2 shows a picture of the setup for the compression tests. Digital Image Correlation (DIC) technique was used to capture the strain field. It is not reliable to record the strain field by simply using the displacement data from the crosshead, due to the compliance of the MTS testing system. A high speed digital camera, XS-4 from IDT, was used to capture the images during deformation and the WinDIC code with the consideration of both first and second order shape functions (Lu and Cary, 2000) was used to determine the actual deformation field in the specimen, and the actual deformation data was used to make corrections on the data obtained from MTS to determine the Young's modulus.

Figure 2.2 Compression test MTS setup

To determine the effect of temperature on the properties of the material, compressive tests were performed on ϕ3.0"x1.0" samples at four different temperatures: RT, - 23 °C, - 80 °C, - 170 °C. The low temperature environments were achieved using the freezer, dry ice and liquid nitrogen, respectively. For testing at temperature lower than room temperature, each sample was placed under each low temperature condition overnight to reach thermal equilibrium. The strain rate for this testing is relatively high, 10 s^{-1}, to ensure that each test will be conducted in a few seconds and the temperature change during the test was minimal.

2.3 Dynamic Mechanical Analysis

Dynamic Mechanical Analysis (DMA) is a tool to study material energy absorption and dissipation through response to an oscillating force. An ideal elastic material will respond instantaneously to the applied sinusoidal wave. An ideal viscous material will have a response with a phase lag $\pi/2$. For a viscoelastic material, the response will be out of phase by $0 \sim \pi/2$ comparing to the applied force. Figure 2.3 shows a typical curve of applied force and material response. Normally the material response in term of displacement will lag behind the applied force. In Figure 2.3 F_d is dynamic oscillatory force, F_s is the static or clamping force. The force, displacement and phase angle, δ, are used to determine the storage modulus, E', and loss modulus, E".

$E' = (f_0 / b\ k) \cos \delta$

$E'' = (f_0 / b\ k) \sin \delta$

$\tan \delta = E''/ E'$

where f_0 = peak value of the sinusoidal force

k = peak value of material response

b = sample geometry factor

δ = phase angle

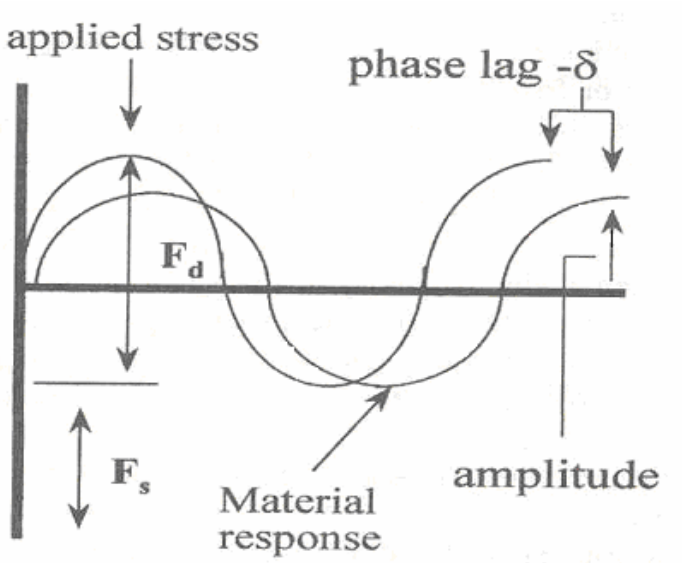

Figure 2.3 Typical DMA oscillating force and material response (Menard, 1999)

Loss tangent indicates the extent of dissipation of energy due to molecular rearrangement and internal friction. The loss modulus indicates the energy loss due to internal friction and other internal motion. The storage modulus shows the ability of the material to return to its initial state after deformation.

DMA allows the user to find the properties within a much shorter time frame than the traditional approach. The complex modulus can be obtained each time the sine wave sweeps. If the test was conducted with varying temperature at the rate of 10 °C /min, the DMA can record the modulus as a function of temperature over 100 °C in 10 minutes. In the traditional method, we have to conduct the experiments at each temperature to

measure the properties. For measuring modulus as a function of temperature, that would require heating the sample to a temperature, equilibrating, performing the experiment, loading a new sample and repeating the tests. To conduct experiments over the temperature range over 100 °C would take days of work.

In the case where the DMA was used to measure the glass transition temperature, such as α transition, of the foam. DMA is more sensitive to determine various transitions than other methods, for example, Differential Scanning Calorimeter (DSC), or the Differential Thermal Analyzer (DTA). Glass transition temperature is a very important property, and for some material that is the upper temperature limit in application. When the material undergoes transition from a hard glassy state to a rubbery state, its physical properties will change dramatically. The method to determine glass transition temperature, T_g, is controversial. This is not unusual as DSC has multiple methods too. Depend on both the industry need and operator's preference, the transition can be determined at the peak of

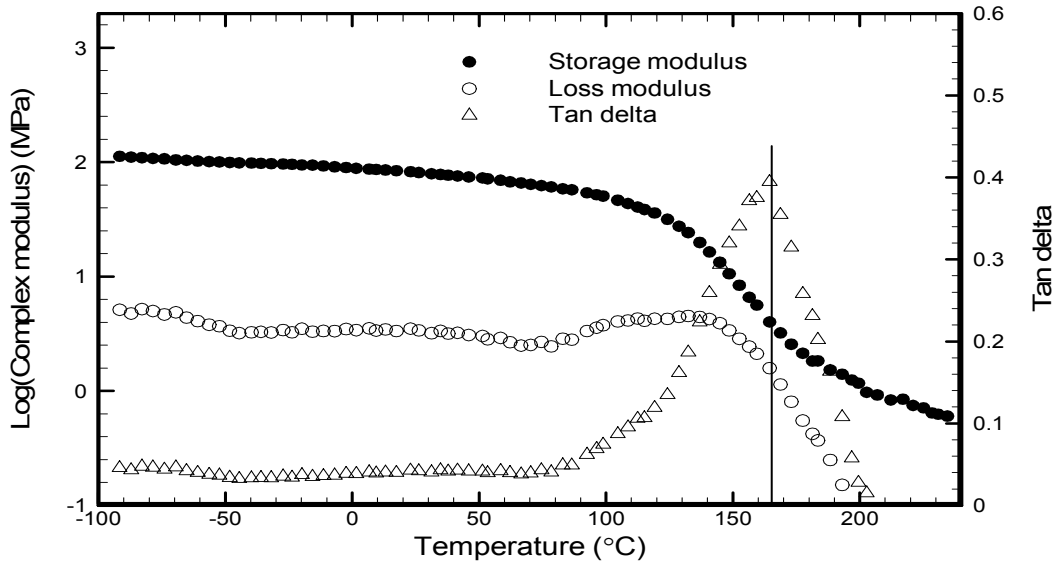

Figure 2.4 Complex modulus (E′, E") and loss tangent of foam from DMA tests

the tangent delta, loss modulus E" and storage modulus E'. The results can sometimes differ by as much as 25 °C for the same test. In our case the glass transition temperature was determined from the peak of the tangent data.

The DMA test result is shown in Figure 2.4.The glass transition temperature, $T_{g,}$ is determined as 165 °. Roughly one third of the energy was lost duo to molecular rearrangement and internal friction, and it proves the foam is a viscoelastic material.

2.4 Digital image correlation method

Digital image correlation (DIC) is a non contact, full field surface strain measurement method. A group of researchers at university of South Carolina (Peters et all, 1982; Sutton et al, 1983) first introduced DIC technique to measure surface deformation. Others have refined this method and extended its application (Vendroux et al, 1994; Lu, et al, 1997; Lu and Cary, 2000). The algorithm used for this study was developed by Lu and Carry (2000), which was capable of measuring both first and second order deformations. It has been shown to be more accurate to measure large nonlinear deformation because of nonlinearity involved in deformation. DIC technique uses a distinct grayscale pattern as a media to correlate a pair of images, before and after deformation, to measure the displacement field. Figure 2.5 shows a typical speckle pattern used in DIC. The

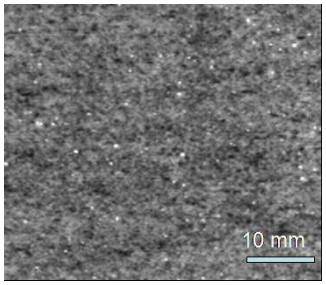

Figure 2.5 Typical pattern for DIC Application

resolution of the measurement is determined by the optical lens and the resolution of the film, or the digital camera.

The strain field was derived from crosshead speed in the MTS testing system**.** Because of the compliance of the various parts in the testing system and the linear range of the foam is very small, the Young's modulus calculated directly from the MTS results is not accurate. To improve accuracy, the digital image correlation technique was used to correct the young's modulus data from MTS. Figure 2.6 shows the differences between MTS and DIC results for the same test. The average value from five tests was used to obtain the correlation factor, which was determined as 1.75, by correlating the MTS and DIC results. The factor was used to make correction for the Young's Modulus obtained from MTS testing data.

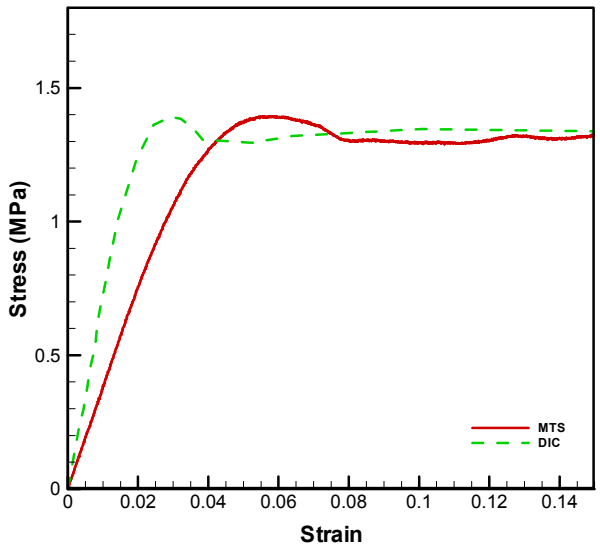

Figure 2.6 Comparison of results from MTS and DIC

Figure 2.7 shows DIC images at different deformation stage. The speckle pattern was created by covering the sample with a thin layer of black ink. At 10 s, it is seen that the sample became slightly shorter, but the speckle pattern did not show much difference. At 20 s the speckle pattern showed significant distortion and the sample became even shorter.

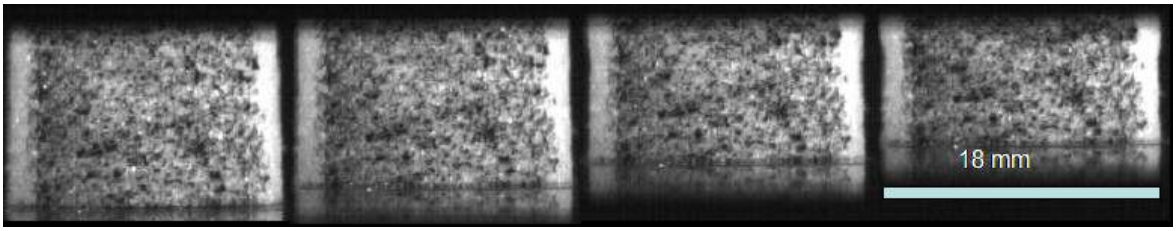

0 s 10 s 20 s 30s

Figure 2.7 DIC images at different deformation stage

At 30 s the sample distorted further and showed large deformation. In this experimental setup, the upper surface was kept stationary and the load was applied from the bottom. The bottom part began to compact first and the compaction wave moved gradually to the top. The behavior can also be verified from the deformation and strain field contour plot in Figure 2.8.

From the DIC images at different stages of deformation, we observed the complexity of foam deformation, which posed a well established challenge in the calculation of material properties. The deformation and strain field are plotted in Figure 2.8. The deformation in the x direction is much smaller than that in the y direction so that the uniaxial stress state has been achieved. The deformation is heterogeneous on the surface.

To determine the minimum size of the representative volume element, the results from different subset sizes for the same test are shown in Figure 2.9. For subset of 20 ~ 40 pixels, the results tends to be consistent, but the data are scattered, which additionally proves that the deformation is heterogeneous. From Figure 2.9, the RVE is determined to be 20×20×20 pixels, or 2.2×2.2×2.2 mm (One pixel is equal to 0.11mm). The sample size used in the experiment should be larger than the size of the RVE to ensure that the results are representative of the average of the material.

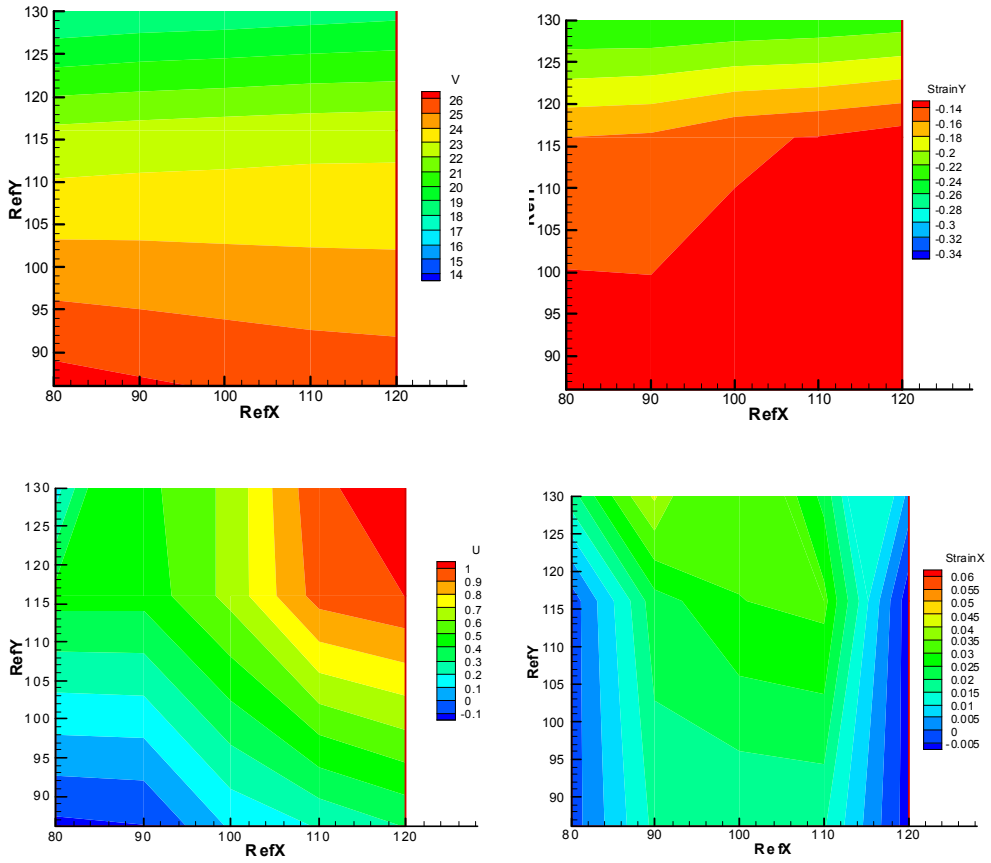

Figure 2.8 Deformation and Strain field (1 pixel=0.11 mm)

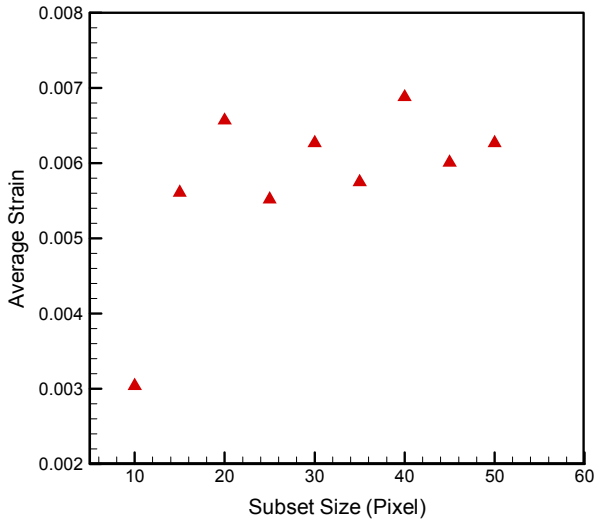

Figure 2.9 Subset size and strain relation (I pixel =0.11 mm)

2.5 Strain Rate Effect

A typical compressive stress-strain curve of the foam is shown in Figure 2.10, which indicates that the foam is a nonlinear material. The material is linear at low stress and

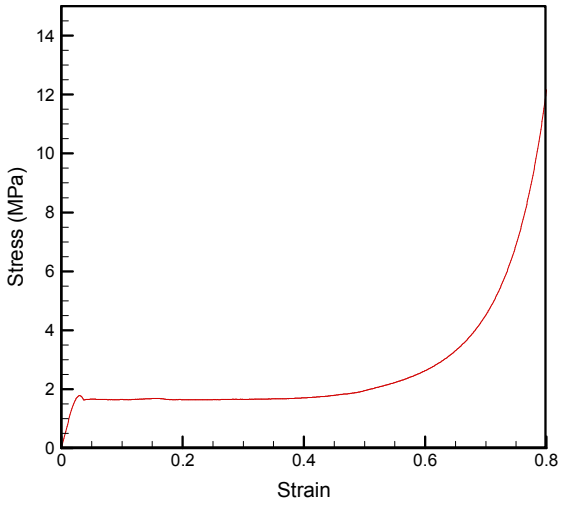

Figure 2.10 Stress strain curve up to 80% compressive strain

reaches its collapse strength at about 2.5% strain, then enters a long plateau region associated with compaction, and begins to harden at about 45% compressive strain. The linear elastic region is controlled by cell wall bending and the plateau is associated with the collapse of the cell by formation of plastic hinges. When the cells almost collapsed completely, the opposing cell wall will touch each other, and further compression will lead to large stress increase.

The stress-strain relations under quasi static state with strain rates ranging from 10^{-3}/s to 10^{1}/s, at room temperature and cryogenic temperature, are shown in Figures 2.11 ~ 2.14. Figure 2.11 and Figure 2.12 show the out-of-plane compressive response. Figure 2.13 and Figure 2.14 show the in-plane properties. Four to five tests were repeated at each strain rate and each temperature. In general, the Young's modulus and the yield strength increase with the increasing of strain rate. However, the Young's modulus data are scattered. The Young's Modulus data are calculated from data corrected using the DIC. The DIC results are directly affected by the grayscale in the image. Different images give slightly different results. The Young's modulus shown here should be considered as an approximation. Table 2.1 lists the compression results, which include the Young's modulus and collapse strength, at room temperature and Table 2.2 lists data at about − 170 °C.

The results indicate that the Young's modulus and collapse strength increase with the increasing of the strain rate. Comparing out-of-plane results at room temperature with strain rates 10^{-3}/s and 10^{1}/s, the Young's modulus increases from 65.97 MPa to 94.10

MPa, which is about 43% of increase from strain rate 10^{-3} /s to 10^{1}/s. The collapse strength creases from 1.44 MPa to 2.01 MPa, which is about 40% of increase within the same strain rates.

We observed a similar trend for the in-plane properties. Comparing in-plane results at room temperature within strain rates 10^{-3}/s and 10^{1}/s, the Young's modulus increases from 74.38 MPa to 91.50 MPa, which is about 23% of increase at 10^{1}/s. The collapse strength increases from 1.64 MPa to 2.26 MPa, which is about 38% of increase.

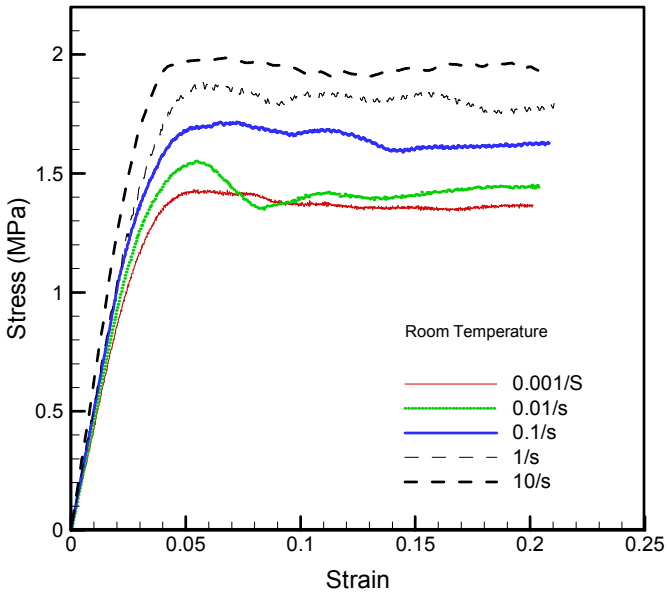

Figure 2.11 Out-of-plane stress strain curves at room temperature

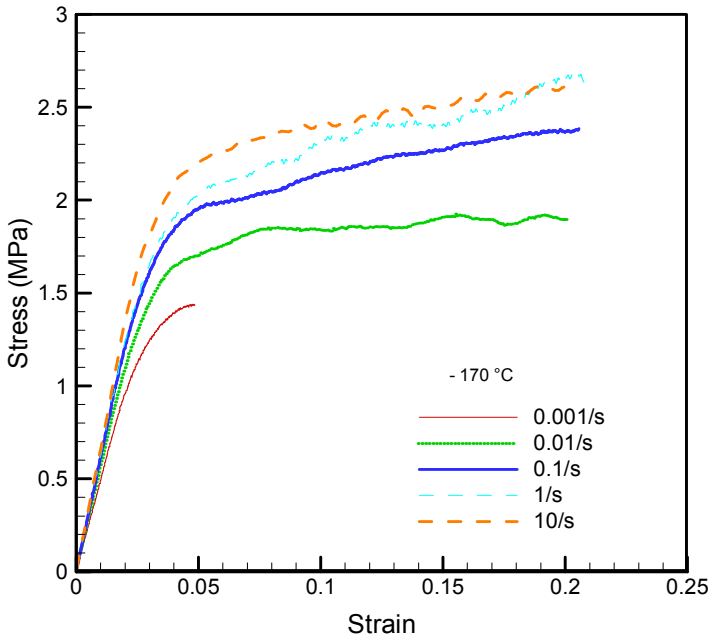

Figure 2.12 Out-of-plane stress strain curves at -170 °C

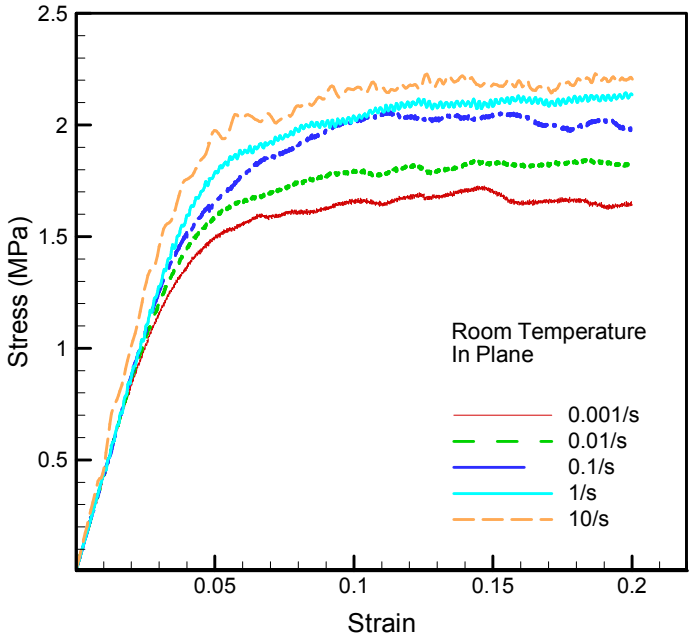

Figure 2.13 In-plane stress strain curves at room temperature

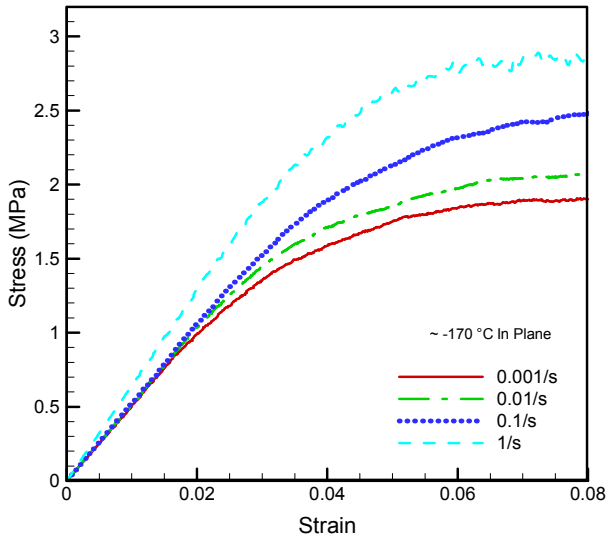

Figure 2.14 In-plane stress strain curve at ~ - 170 °C

Table 2.1. Compression data at room temperature

23 °C			
Testing	Strain Rate (1/s)	Young's Modulus (Mpa)	Collapse Strength (Mpa)
Out-of-plane	0.001	65.97±1.52	1.44±0.01
	0.01	72.69±3.11	1.56±0.04
	0.1	76.14±1.02	1.76±0.03
	1	80.19±1.53	1.86±0.02
	10	94.10±4.41	2.01±0.03
In-plane	0.001	74.38±2.21	1.64±0.06
	0.01	74.95±0.78	1.87±0.78
	0.1	81.57±3.08	2.14±0.06
	1	82.78±6.35	2.17±0.13
	10	91.50±6.72	2.26±0.03

Table 2.2. Compression data at ~ -170 °C

- 170 °C			
Testing	Strain Rate (1/s)	Young's Modulus (Mpa)	Collapse Strength (Mpa)
Out-of-plane	0.001	75.96±3.90	/
	0.01	86.67±3.77	1.83±0.07
	0.1	94.89±1.36	2.13±0.07
	1	96.83±2.52	2.20±0.01
	10	102.08±5.14	2.29±0.04
In-plane	0.001	87.87±1.96	/
	0.01	91.40±0.84	2.19±0.10
	0.1	95.58±4.14	2.67±0.10
	1	109.84±4.16	2.73±0.24
	10	101.22±3.31	2.76±0.2

compression results show that both in-plane and out-of-plane properties, Young's modulus and collapse strength, are affected by the strain rate. The relationship between collapse strength and stain rate can be fitted into an analytical solution developed by Chen and Zhou (1995).

$$\frac{\sigma_y}{\sigma_0} = 1 + \frac{2}{\pi} C_1 \tanh[\ln(\frac{\dot{\varepsilon}}{\dot{\varepsilon}_0})^m]$$

where σ_y is the collapse strength, σ_0 is a reference compressive strength, C_1 is the amplitude coefficient of the collapse strength, m is the stain rate factor. And $\dot{\varepsilon}_0$ is the strain rate at the turning point within a medium strain rate range, usually ~ 100 /s. The fitted constants for both in-plane and out-of-plane properties at both room and cryogenic temperatures are listed in Table 2.3. The fitted curves along with the experiment data are plotted in Figure 2.15 ~ 2.16. Figure 2.15 shows the fitted results from out-of-plane data while Figure 2.16 shows fitted results for the in-plane data. The fitted curve agrees very well with the experiment data.

Table 2.3 Fitted constants for collapse strength

$\dot{\varepsilon}_0$ =100		σ_0	C_1	m
Out-of-plane	RT	0.47	0.59	0.07
	- 170 °C	0.42	0.6	0.04
In-plane	RT	0.42	0.6	0.04
	- 170 °C	0.35	0.4	0.04

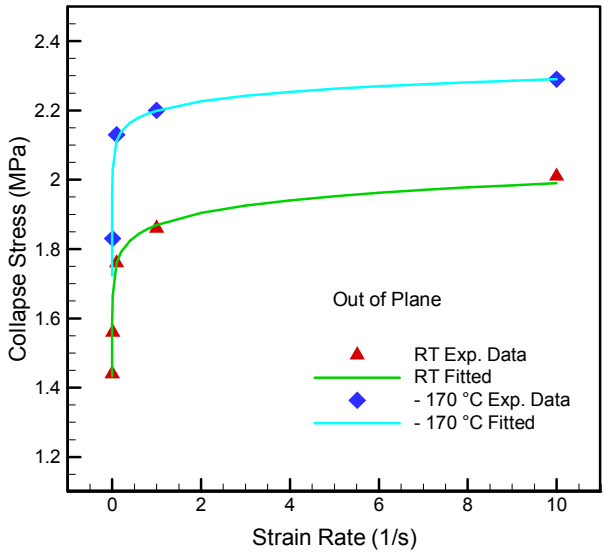

Figure 2.15 Out-of-plane collapse strength as a function of strain rate

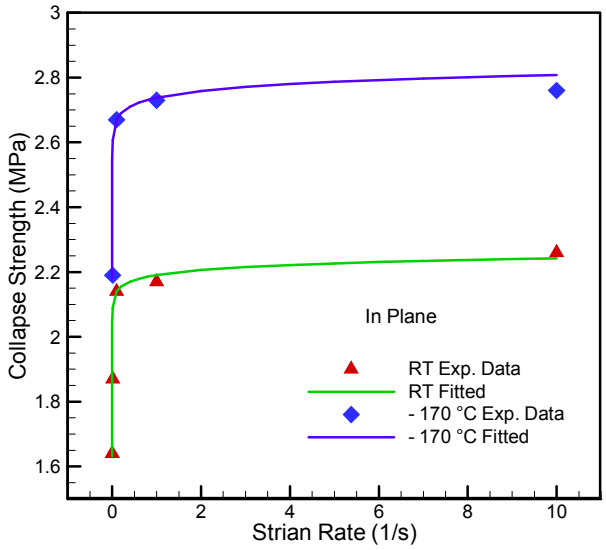

Figure 2.16 In-plane collapse strength as a function of strain rate

The Young's modulus shows a linear relation with the logarithm of the strain rate and is fitted into the following equation

$$E = A \, \mathrm{Log}(\dot{\varepsilon}) + E_0$$

where the Young's modulus, $E_{0,}$ is a reference Young's modulus, A is a constant. The fitted constants are listed in Table 2.4. Figure 2.17 and Figure 2.18 show the fitted Young's modulus curve with both the in-plane and out-of-plane data. The fitted curve shows the same trend with the experimental results, but does not agree well with the experimental data.

Table 2.4 Fitted constants for Young's Modulus

		A	E_0
Out-of-plane	RT	6.38	84.19
	- 170 °C	6.24	97.53
In-plane	RT	4.21	85.24
	- 170 °C	4.51	101.70

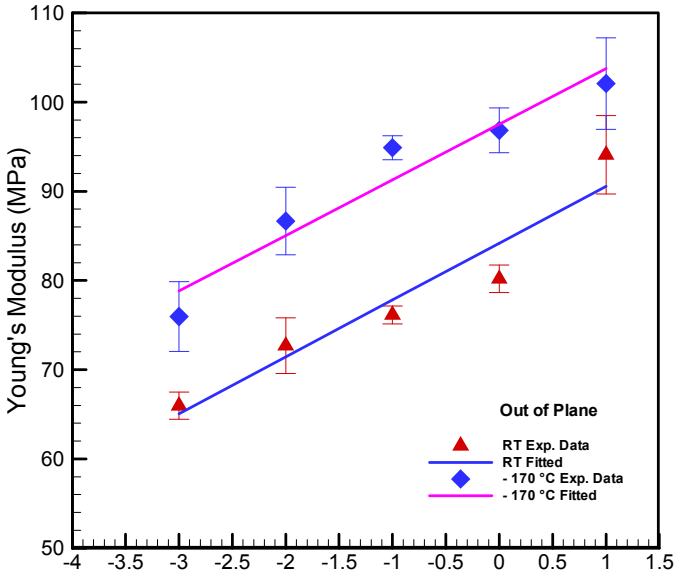

Figure 2.17 Out-of-plane Young's modulus and strain rate relation

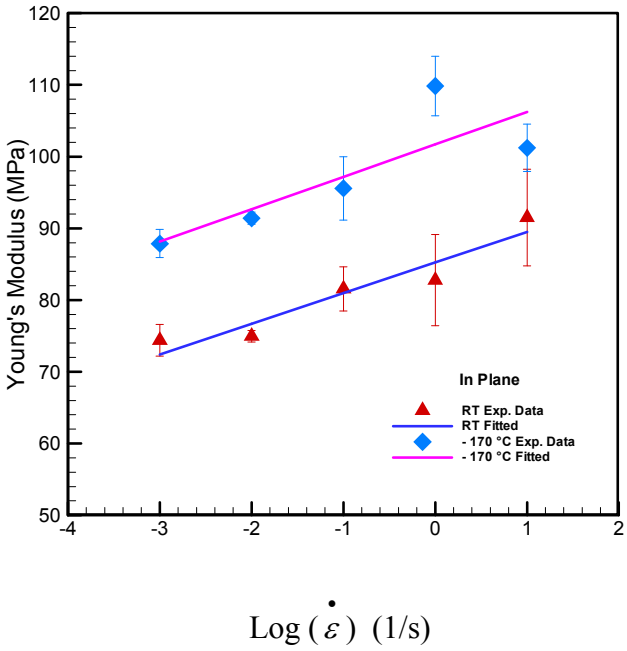

Figure 2.18 In-plane Young's modulus and strain rate relation

2.6 Temperature Effect

To investigate the effect of temperature on the compressive behavior of the foam, compressive tests were conducted at four different temperatures: RT, - 23 °C, - 80 °C, - 170 °C. The stress-strain-curves at these four different temperatures are shown in Figure 2.19. The data are listed in Table 2.5. The collapse strength is higher at lower temperature. The Young's modulus is not sensitive to temperature change between - 80 °C and 23 °C, but is much higher at about - 170 °C.

Overall, temperature has some effects on the results. The Young's modulus and collapse strength at low temperature are higher than those at room temperature. For example, at strain rate 10^{-2}/s, the Young's modulus at − 170 °C increases by 19% and the collapse

strength increases by 17% comparing to data at room temperature. The effect of temperature should also be considered during the design process.

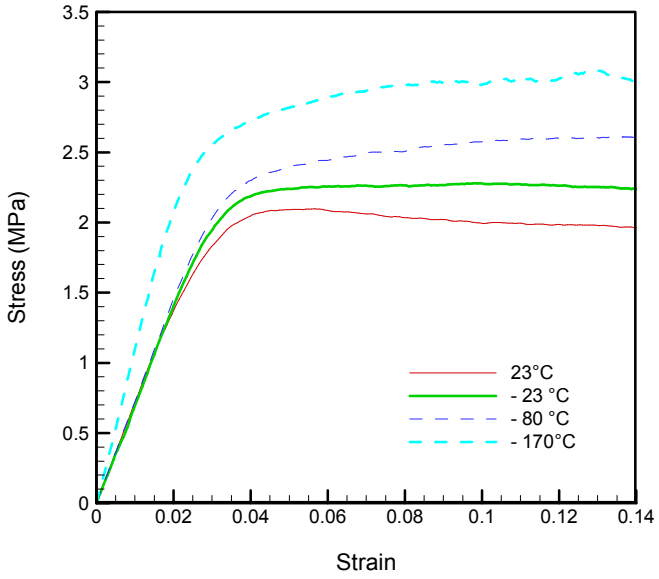

Figure 2.19 Stress strain curve at different temperatures

Table2.5 Young's Modulus and Collapse Strength at different temperatures

Temperature(°C)	E(Mpa)	Yield Stress (Mpa)
23	78.433±2.856	1.7±0.1
-23	70.112±0.662	1.85±0.05
-80	72.577±1.539	2.0±0.1
-170	109.624±2.207	2.15±0.05

CHAPTER III

RELAXATION BEHAVIOR

3.1 **Relaxation Experimental Setup**

For a viscoelastic material, low temperature response will be similar to the short term response. Relaxation tests at low temperature were carried out using ϕ3"x3" sample. Figure 3.1 shows the relaxation setup at low temperature. The MTS testing system was also used for relaxation compressive test. A low temperature environment was generated by injecting liquid nitrogen into a foam chamber.

Figure 3.1 Low temperature Relaxation test set up

The metal part of the MTS inside the foam chamber was wrapped with plastic foam to slow down the heat transfer process so that the sample can reach thermal equilibrium

faster and keep the temperature approximately constant during each relaxation test. Through controlling the flow rate of the liquid nitrogen, the temperature in the foam chamber can be set to at a certain temperature. The variation is less than two degrees. The relaxation tests were performed at five different temperatures: -165 °C, -125 °C, -82 °C, -42 °C, RT. A silicon diode temperature sensor as shown in Figure 3.2a with Omega CyC3200 temperature controller as shown in Figure 3.2b was used to measure the temperature. The application range of the temperature sensor varies from 1.4 to 475K and the accuracy is ±1.5K.

a) b)

Figure 3.2 a) Silicon diode temperature sensor, b) Temperature controller

3.2 **Relaxation Master Curve**

Relaxation tests were carried out at five different temperatures using ϕ3"x3" cylindrical samples. For purpose of comparison with data from compression on ϕ0.7"x0.5" samples, the results were modified using the correlation factor of compression data between ϕ3"x3" and ϕ0.7"x0.5" cylindrical samples and the modified results are plotted in Figure 3.3. The relaxation master curve, as shown in Figure 3.4, is obtained from test results at different temperatures based on time-temperature superposition principle. Figure 3.5

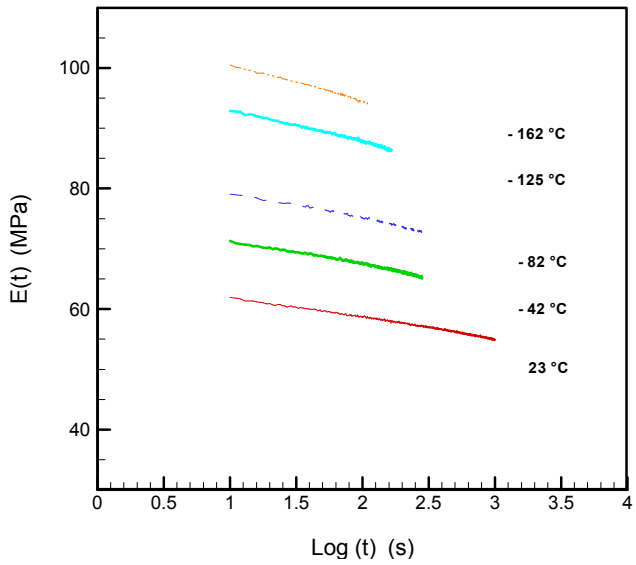

Figure 3.3. Relaxation modulus at five different temperatures

shows the shift factor. Extrapolation is used to fill the gaps in the mastercurve. The relaxation modulus decreases nearly linearly over the logarithm of time. To fill the gap, tests at more temperatures will be needed. But, the extrapolated master curve does not appear to affect our understanding of the material relaxation behavior. The results indicate that over ten years of service life, the properties of the foam will change gradually. Since the master curve was constructed based on the test results at low temperature, it is suggested that the properties at room temperature need to be used in engineering design. The Young's relaxation modulus is fitted into a 11 terms Prony series, as shown in Figure 3.4,

$$E(t) = E_{\inf} + \sum_{i=1}^{11} E_i * Exp(-t * \lambda_i) \text{ MPa}$$

where t is time in second, λ is the reciprocal of relaxation time τ , $\lambda = 1/\tau$. E_{inf} if the long term modulus. From the master relaxation modulus, the Young's modulus is expected to reduce by ~45% over twenty years. The long-term relaxation modulus is ~55 MPa.

Table 3.1 Prony series coefficients

E_{inf} = 54.95 MPa	
E_i (MPa)	λ_i (1/s)
1.92	1.00E-03
4.89	1.00E-02
1.70	1.00E-01
6.02	1.00E+00
2.48	1.00E+01
5.49	1.00E+02
3.14	1.00E+03
6.61	1.00E+04
4.11	1.00E+05
6.57	1.00E+06
5.21	1.00E+07

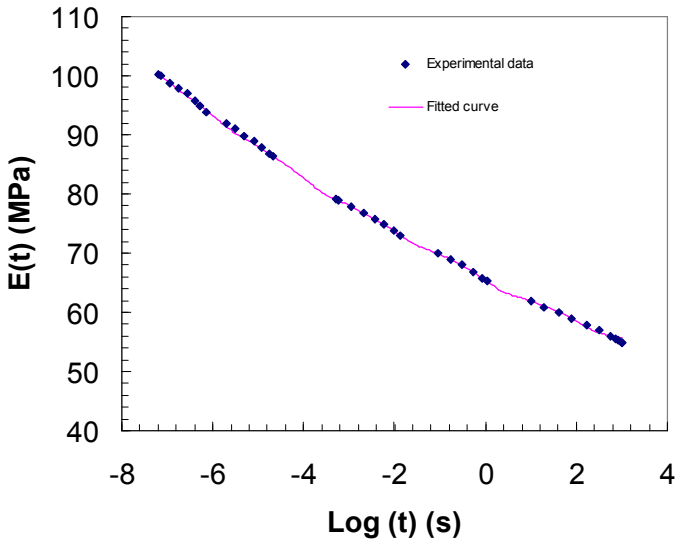

Figure 3.4 Relaxation master curve (Extrapolations are used to fill gaps between neighboring curves)

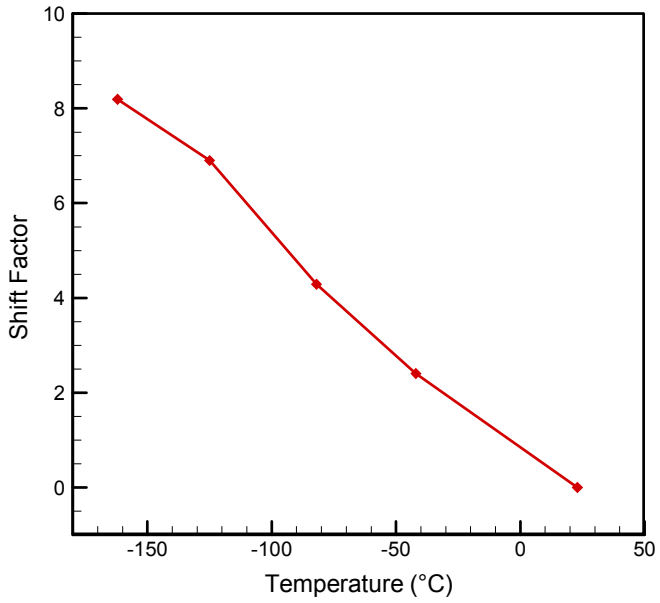

Figure 3.5 Shift factor refer to room temperature

3.3 Comparison Young's Modulus from Compression and Relaxation Experiments

From the average young's modulus data, the Young's modulus can be fitted into Prony series using a method described below.

For a linear viscoelastic material under uniaxial stress state, the stress, σ, can be determined from the applied strain history, ε (t), using

$$\sigma(t) = \int_0^t E(t-\xi)\frac{d\varepsilon(\xi)}{d\xi}d\xi \,. \qquad (1)$$

where E(t) is the Young's relaxation modulus

At a constant strain rate, $\dot{\varepsilon}(t) = \dot{\varepsilon}_0$, Eq. (1) becomes

$$\sigma(t) = \dot{\varepsilon}_0 \int_0^t E(\xi) d\xi \tag{2}$$

Eq. (2) can be written as

$$\frac{\sigma(t)}{\varepsilon(t)} = \frac{1}{t} \int_0^t E(\xi) d\xi = \overline{E}(t) \tag{3}$$

where $\overline{E}(t)$ is the average uniaxial relaxation modulus from time 0 to *t*. Eq. (3) indicates that the average Young's modulus is equal to the ratio of stress to strain under constant strain rate history. On the other hand, taking derivative of Eq. (2) with respect to *t*, one has

$$\frac{d\sigma(t)}{\dot{\varepsilon}_0 dt} = E(t), \text{ i.e., } \frac{d\sigma}{d\varepsilon} = E(t) \tag{4}$$

Eq. (4) implies that under constant strain rate history, $E(t)$ is equal to tangent modulus. For a viscoelastic material, the uniaxial relaxation modulus can be represented by the generalized Maxwell model,

$$E(t) = E_\infty + \sum_{i=1}^{N} E_i e^{-t/\tau_i} \tag{5}$$

Substituting Eq. (5) into Eq. (2) leads to

$$\sigma(t) = \dot{\varepsilon}_0 \left[E_\infty t + \sum_{i=1}^{N} \tau_i E_i (1 - e^{-t/\tau_i}) \right] \tag{6}$$

At constant strain rate, Eq. (6) can be written as

$$\sigma(t) = \varepsilon(t) E_\infty + \dot{\varepsilon}_0 \sum_{i=1}^{N} E_i \tau_i \left[1 - e^{-\varepsilon(t)/(\tau_i \dot{\varepsilon}_0)} \right] \tag{7}$$

Eq. (7) can also be written as

$$\bar{E}(t) = \frac{\sigma(t)}{\varepsilon(t)} = E_\infty + \sum_{i=1}^{N} E_i \frac{\tau_i}{t}\left[1 - e^{-t/\tau_i}\right] \tag{8}$$

Therefore, given the relaxation function for a viscoelastic material, the stress-strain data at a constant strain rate can be determined. On the other hand, if the stress-strain data are given at a constant strain rate, they can be fitted into Eq. (7) to find the best-fit parameters E_i, τ_i for use in Eq. (5) to determine the relaxation modulus. Using Eq. (8) and consider only one exponential term, as in the case of a standard linear solid model, the average uniaxial relaxation modulus is given as

$$\bar{E}(t) = \frac{\sigma(t)}{\varepsilon(t)} = E_\infty + E_1 \frac{\tau}{t}\left[1 - e^{-t/\tau}\right]. \tag{9}$$

Eq. (9) is used to fit measured average modulus within the range of strain between 0 to 1% under different strain rates. The best-fit parameters E_∞, E_1 and relaxation time $\tau = 10^{-5}$ will be used to determine the Young's relaxation modulus $E(t)$, in the form of Eq. (5) with the consideration of one exponential term, is

$$E(t) = E_\infty + E_1 e^{-t/\tau} \text{ MPa} \tag{10}$$

Figure 3.6 shows the comparison of the Young's modulus from compression test with that from relaxation. The detail data are listed in table 3.2. It shows the results from relaxation tests agree reasonably well with compressive data. The biggest difference is within 20%.

Table 3.2 Comparing data from Relaxation and compression test.

Strain Rate (/s)	t (s)	Relaxation (Mpa)	Compression (Mpa)	Difference (Er-Ec)/Er %
0.001	10	62.01	65.97	6.38
0.01	1	65.74	72.69	10.57
0.1	0.1	69.70	76.14	9.23
1	0.01	73.92	80.19	8.47
10	0.001	78.42	94.1	20.00

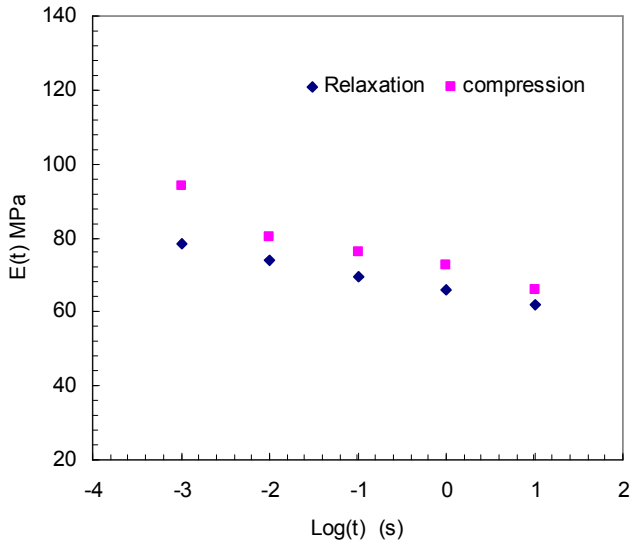

Figure 3.6 Comparison results from compressive and relaxation

CHAPTER IV

FRACTURE TOUGHNESS

4.1 Fracture Experiment Set up

In order to find the ability of the foam to resist the propagation of cracks, the fracture toughness will be measured. The same material as used in compressive tests, was used to characterize the facture toughness. According to the fracture toughness testing standard ASTM D5045-99, the single-edge-notch bending (SENB) sample as shown in Figure 4.1 was prepared in the Polymer Mechanics Lab at Oklahoma State University. A crack was

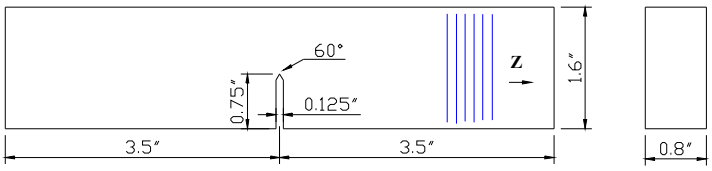

Figure 4.1. Notched three-point bending sample

initiated in the rectangular block sample by using a saw to cut a notch first and then using a razor blade to cut a sharp crack following the standard. The crack was parallel to the plane of the fiber and the fracture toughness determined from this direction will be the

minimum value. All samples were cut using a band saw and polished with a sand paper after machining to generate smooth surface for testing. The experiments were conducted at room temperature (22±1°C) and relative humidity 23±1%.

An MTS three-point bending fixture as shown in Figure 4.2 was used on an Instron screw-driven test system to measure the fracture toughness of the material. The loading direction was the same as the crack direction. The crosshead speed was maintained at constant speed 0.17 mm/s during the test.

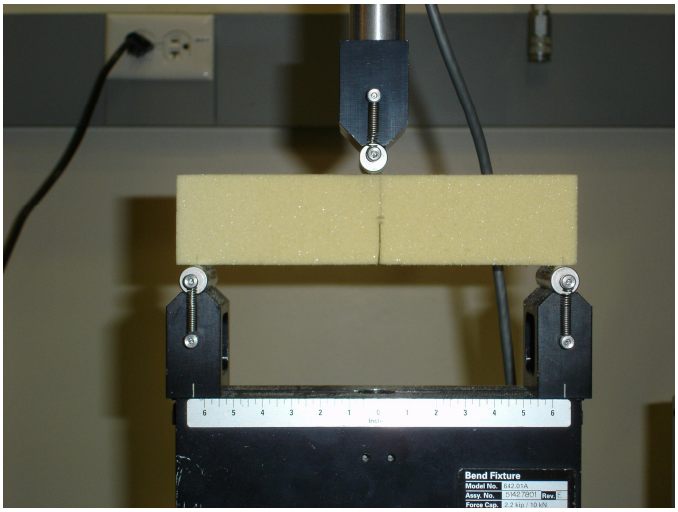

Figure 4.2 Three-point bending fixture

4.2 Fracture Toughness

The fracture toughness and critical energy release rate for SENB sample with crack aligned in the fiber direction were calculated according to ASTM D5045-99.

$$K_Q = (\frac{P_Q}{BW^{1/2}}) f(x)$$

$$f(x) = 6(x)^{1/2} \frac{[1.99 - (x)(1-x)(2.15 - 3.93x + 2.7(x)^2]}{(1+2x)(1-x)^{3/2}}$$

$$G_Q = U/(BW\phi)$$

$$\phi = \frac{A + 18.64}{dA/dx}$$

$$A = [16x^2/(1-x)^2][8.9 - 33.717x + 79.616x^2 - 112.952x^3 + 84.815x^4 - 25.672x^5]$$

$$dA/dx = [16x^2/(1-x)^2]\{[-33.717 + 159.232x - 338.856x^2 + 339.26x^3 - 128.36x^4] + 16[8.9 - 33.717x + 79.616x^2 - 112.952x^3 + 84.815x^4 - 25.672x^5][x(1-x) + 2x^2]/(1-x)^3\}$$

where

K_Q = Fracture toughness, or stress intensity factor, MPa.m$^{1/2}$

P_Q = Peak Load, KN

B = Specimen thickness, cm

W = Specimen depth, cm

a = Crack length, cm

G_Q = Critical Energy Release Rate, KJ/m^2

U = corrected Energy

x = a/W

The critical stress intensity factor is determined as 110.25±8.39 Kpa.m$^{1/2}$ and the critical energy release rate is 22.25±4.86 J/m^2. These are the average values from four tests. The load-displacement curves of four tests under the same condition for fracture toughness

testing are shown in Figure 4.3. Figure 4.4 shows the fractured sample and the fracture surface.

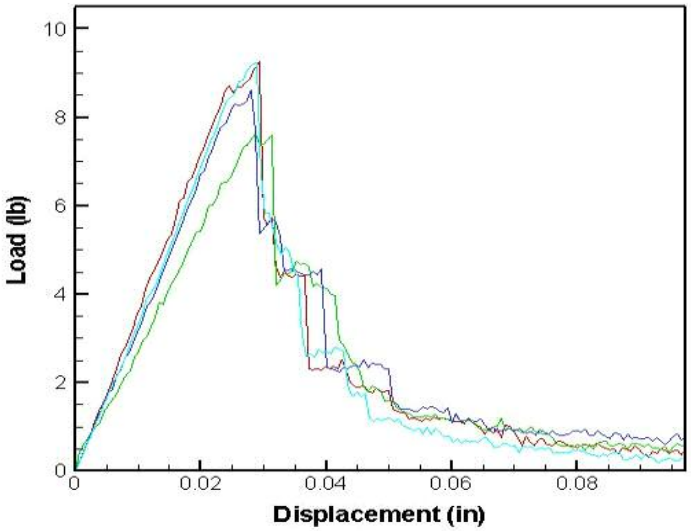

Figure 4.3 Load-displacement curves for fracture toughness testing

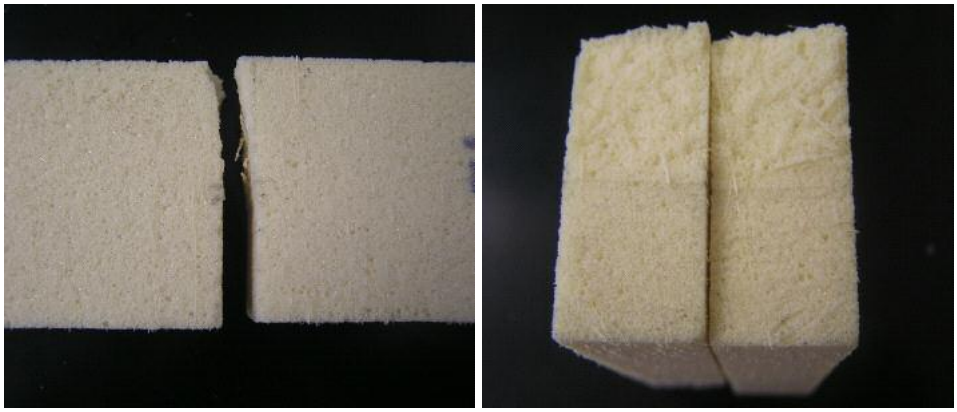

(a) (b)

Figure 4.4. (a) Fractured sample (b) Fracture surface

CHAPTER V

RESIDUAL TENSILE STRENGTH

5.1 Residual Tensile Strength Experiment Setup

The dog-bone shaped sample, revised from tensile sample in ASTM D1623-03 for rigid cellular plastics, was used to measure the residual tensile strength after repetitive compression. The detailed drawing of the sample is shown in Figure 5.1. The samples were machined by JZ systems using water-jet cutting and polished with a sand paper after machining to generate smooth surface for testing. Experiments were performed at room temperature at (23±1°C) and relative humidity 55±5%.

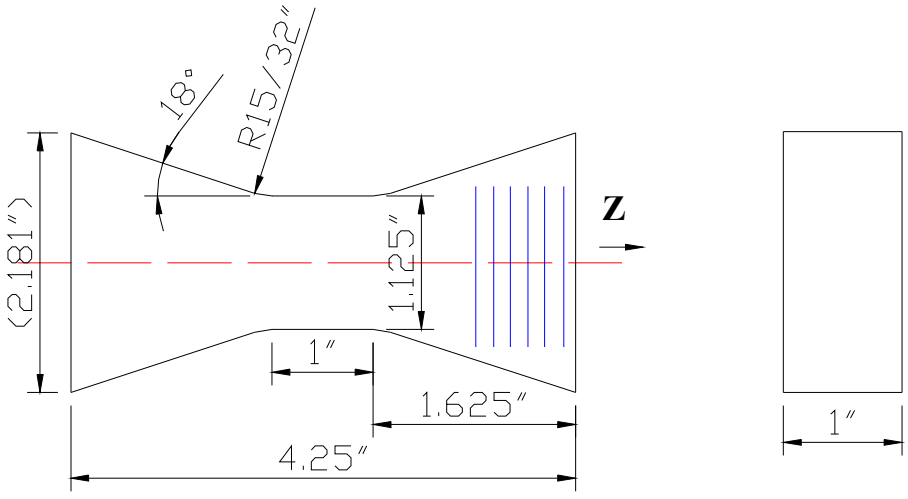

Figure 5.1 Detail drawing of dog-bone shape sample

To perform the residual tensile test, a fixture was made to hold the dog-bone shaped sample. The same MTS system as the compression test with this fixture was used to perform this test. Figure 5.2 shows a sample on the fixture for measurement of residual tensile strength. The frequency used in this study is 0.5 Hz, which is similar to the LNG sloshing rate in application.

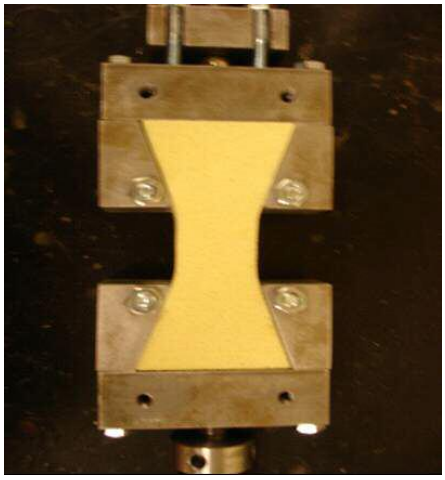

Figure 5.2 Detail residual tensile strength setup

5.2 Residual Tensile Strength

Residual tensile strength under repetitive loading at 1.5% compressive strain was determined at 23 °C. The results are listed in Table 5.1 and shown in Figure 5.3. The values are the average of three tests. This study determined the residual tensile strength after 0, 1, 10, 20, 50,100 cycles of compression. The amplitude of compressive stress in each loading cycle is 0.89 MPa, which is about 55% of the compressive strength. The results in Table 5.1 and Figure 5.3 show that the residual strength after repetitive compression has been reduced. After 100 cycles of repetitive compression, the tensile

strength decreased by 40%. Figure 5.4 shows the tensile fracture surface after being compressed 100 cycles.

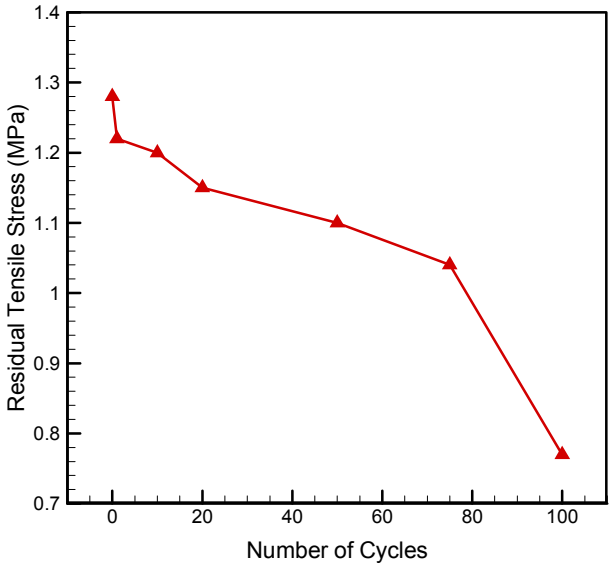

Figure 5.3 Residual tensile strength after repetitive compression

Table 5.1 Residual tensile strength test data

No. of Cycles	Average Stress (MPa)
0	1.28±0.03
1	1.22±0.04
10	1.20±0.01
20	1.15±0.01
50	1.1±0.01
75	1.04±0.06
100	0.77±0.03

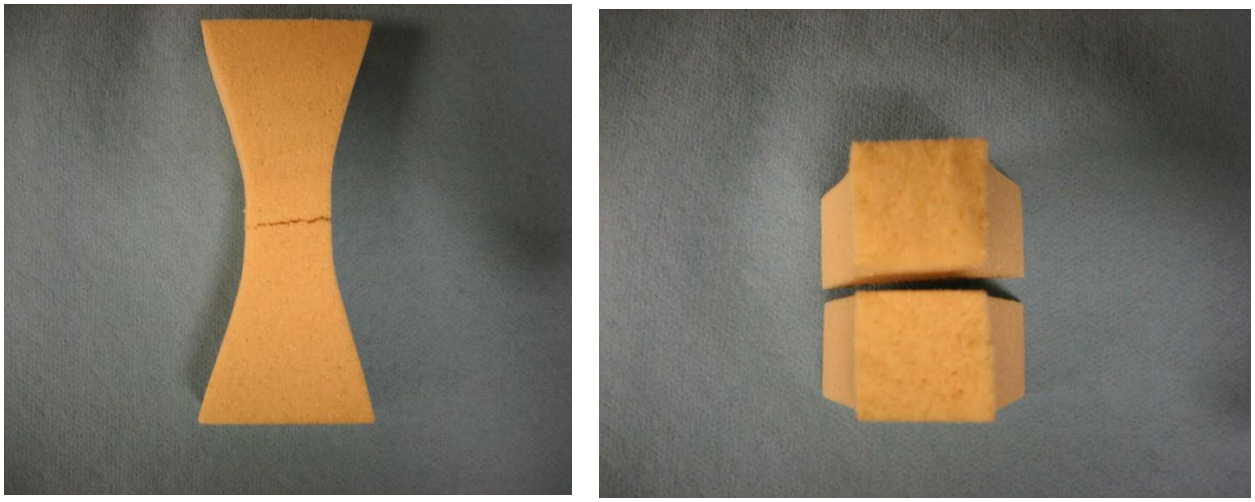

Figure 5.4 Photograph of the fractured surface after being compressed 100 cycles.

CHAPTER VI

CONCLUSION

Compression, fracture toughness, as well as residual tensile strength experiments were conducted to determine the compressive properties. Results indicate that the properties of polyurethane foam depend on temperature and strain rate. Compressive tests for both in-plane and out-of-plane were conducted at five different strain rates, ranging from 10^{-3} /s to 10 /s, and residual tensile strength was carried out at 1.5% strain with 0, 1, 10, 20, 50, 100 compressive cycles. The results showed that Young's modulus and collapse strength increase with the increasing of the strain rate. At room temperature, the Young's modulus and collapse strength are 65.97 Mpa and 1.44 Mpa, respectively, at strain rate 10^{-3}/s, and they are 94.10 Mpa and 2.01 Mpa at strain rate 10/s. These properties also increase at lower temperature. At −170 °C, the Young's modulus and collapse strength are 86.67 Mpa and 1.83 Mpa, respectively, at strain rate 10^{-2}/s; they are 102.08 Mpa and 2.29 Mpa at strain rate 10/s. In design analysis, it is recommended to use 65 MPa as the Young's modulus and 1.44 MPa as the compressive strength of the foam to ensure safety. Young's relaxation master curve obtained based on the results at different temperature shows that the properties of the foam material will change over the service life. From the master relaxation modulus, the Young's modulus is expected to reduce by ~45% over twenty years. The long-term relaxation modulus is ~55 MPa. The fracture toughness is low. The

critical stress intensity factor and critical energy release rates are determined to be 110.25 $KPa.m^{1/2}$ and 22.25 J/m^2, respectively, which indicate that the foam can fail easily when there are in-plane cracks. Tensile strength was reduced rapidly after dozens of compression cycles. Without compressive cycling the tensile strength is 1.28 Mpa. After 100 cycles of compression at the amplitude of 0.89 MPa (55% of the initial compressive strength), the tensile strength is reduces to 0.77 MPa.

REFERENCE

Avci, A., Arikan H. and Akdemir A., 'Fracture behavior of glass fiber reinforced polymer Composite', *Cement and Concrete Research* **34**, 2004, 429-434.

Brydon, A.D., Bardenhagen, S.G., Miller, E.A. and Seidler, G.T., 'Simulation of the densification of real open-celled foam microstructures', *Journal of the Mechanics and Physics of Solids* **53**, 2005, 2638-2660.

Chen, W. and Zhou, B., Constitutive behavior of Epon 828/T-403 at various strain rates, *Mechanics of Time-Dependent Materials* **2**, 1998, 103-111.

Chen, W., Lu F. and Winfree N., 'High-strain-rate compressive behavior of a rigid polyurethane foam with various densities', *Exp. Mech.* **42**, 2002, 65-73.

Choi, S. and Sankar B.V., 'Fracture toughness of carbon foam', *Journal of Composite Materials* **37**, 2003, 2101-2116.

Gama, B.A., Lopatnikov, S.L. and Gillespie, J.W., 'Hopkinson bar experimental technique: A critical review', *Applied Mechanics Reviews* **57**(4), 2004, 223-250.

Gibson, Lorna J. and Ashby, Michael F., 'Celluar Solids, Structure and Properties, 2nd Edition' , *Cambridge University Press*, 1999.

Gray, G.T., 'Classic split-Hopkinson pressure bar technique', *Mechanical Testing and Evaluation*, ASM Handbook **8**, 2000, 462-476.

Kabir, M.E., Saha, M.C. and Jeelani S., 'Tensile and fracture behavior of polymer

foams', *Material Science and Engineering* **429**, 2006, 225-235.

Kyriakides, S., Arseculeratne, R., Perry, E.J., and Liechti, K.M., 'On the compressive failure of fiber reinforced composites', *International Journal of Solids and Structures* **32**, 1995, 689-738.

Landro, LD, Sala G and Olivieri D., 'Deformation mechanisms and energy absorption of polystyrene foams for protective helmets', *Polymer Test* **21**, 2001, 217-228.

Liu, Q., Subhash G. and Gao X.L., 'A parametric study on crushability of open-cell structural polymeric foams', *Journal of Porous Materials* **12**, 2005, 233-248.

Lu, H., Vendroux, G. and Knauss W.G., 'Surface deformation measurements of a cylindrical specimen by digital image correlation', Exp. Mech. **37**, 1997, 433-439.

Lu, H. and Cary, P.D., 'Deformation measurements by digital image correlation: Implementation of a second-order displacement gradient', Exp. Mech. **40**(4), 2000, 393-400.

Luo, H. and Lu, H., 'The compressive behavior of isocyanate-crosslinked silica aerogel at high strain rates', *Mechanics of Time-Dependent Materials* **10**, 2006, 83-111.

Menard, K.P., 'Dynamic mechanical analysis, a practical introduction', *CRC Press*, 1999.

Papka, S.D. and Kyriakides, S., 'In-plane crushing of a polycarbonate honeycomb', *Int. J. Solids Structures* **35**, 1998, 239-267.

Peters, W.H. and Ranson, W.F., 'Digital image techniques in experimental stress analysis', Ppt. Eng. **21**, 1982, 427-432.

Peters, W.H., Sutton, M.A., Ranson, W.F. Poplin, W.P. and Walker, D.M., 'Whole Field Experimental displacement analysis of composite cylinders', Exp. Mech., 1989, 58-62.

Saha, M.C., Mahfuz, H., Chakravarty, U.K., and Uddin, M., Kabir, Md E., and Jeelani, S., 'Effect of density, microstructure, and strain rate on compression behavior of polymeric foams', *Material Science and Engineering* **A 406**, 2005, 328-336.

Song, B., Chen, W., Dou S., Winfree N.A. and Kang J.H., 'Strain-rate effects on elastic and early cell-collapse responses of a polystyrene foam', *International Journal of Impact Engineering* **31**, 2005, 509-521.

Subhash, G. and Liu, Q., and Gao, X.L., ' Quasistatic and high strain rate uniaxial compressive response of polymeric structural foams', *International Journal of Impact Engineering* **32,** 2006, 1113-1126.

Vendrous, G. and Knauss, W.G., 'Deformation measurements at the sub-micron size scale: II Refinements in the algorithm for digital imagecorrelation', *Galcit Report* 94-5, California Institute of Technology, Pasadena

Weiser ES, Johnson TF, Clair TLS, Echigo Y.,Kaneshiro H, Grimsley BW., 'Polyimide Foams for aerospace vehicles', *High Performance Polymer* **12**, 2000, 1-12.

APPENDIX

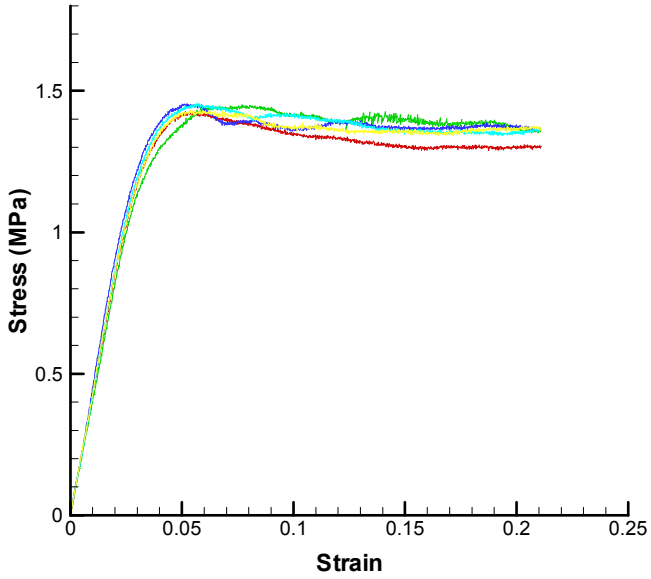

Figure A.1. Quasi-static stress-strain curves of foam at 23 °C at strain rate 0.001 s^{-1}.

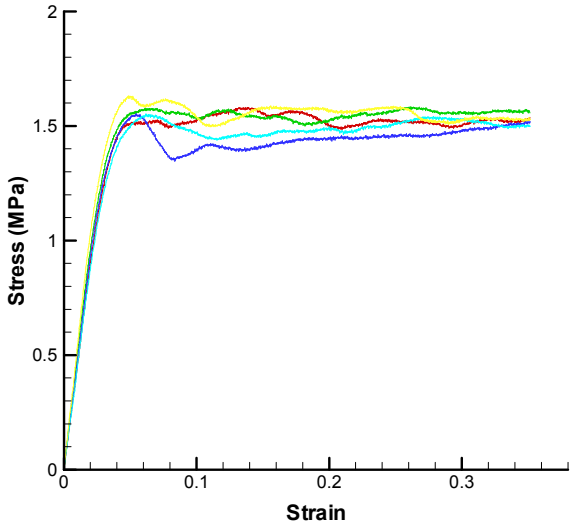

Figure A.2. Quasi-static stress-strain curves of foam at 23 °C at strain rate 0.01 s^{-1}.

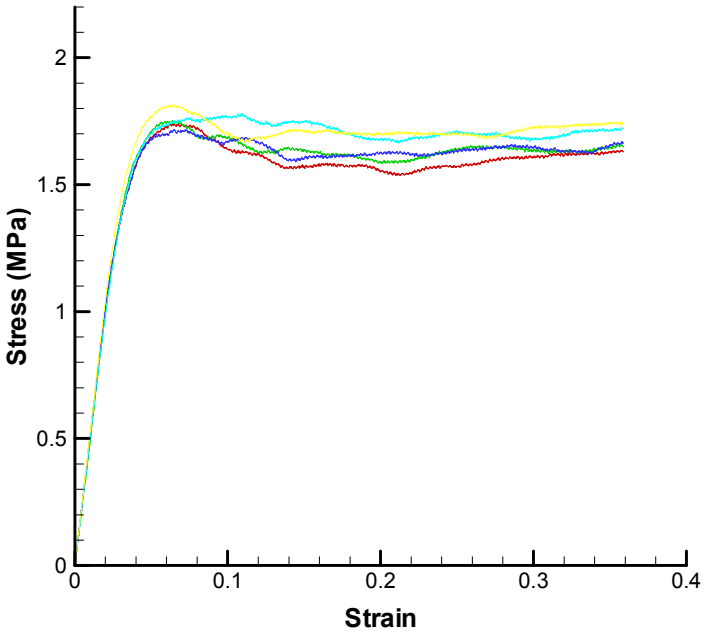

Figure A.3. MTS static stress-strain curves of foam at 23 °C at strain rate 0.1 s^{-1}

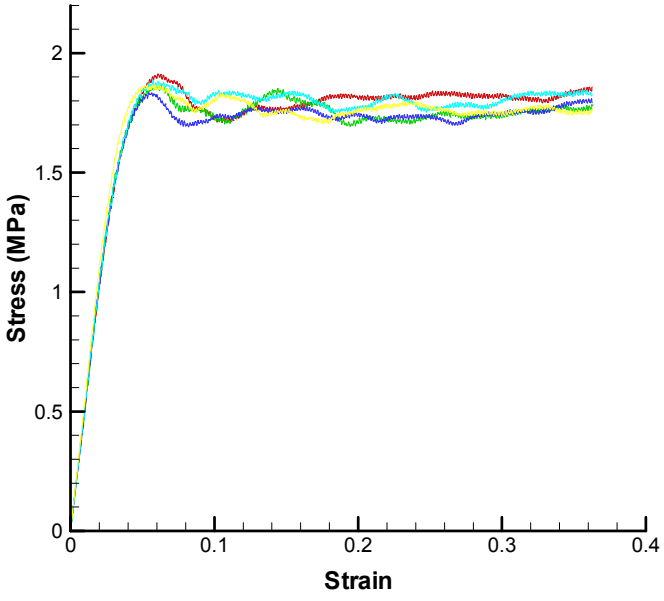

Figure A.4. MTS static stress-strain curves of foam at 23 °C at strain rate 1 s^{-1}

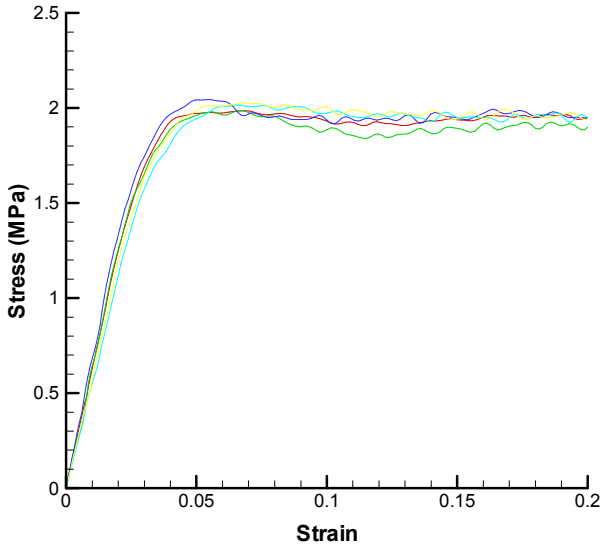

Figure A.5. MTS static stress-strain curves of foam at 23 °C at strain rate 10 s^{-1}

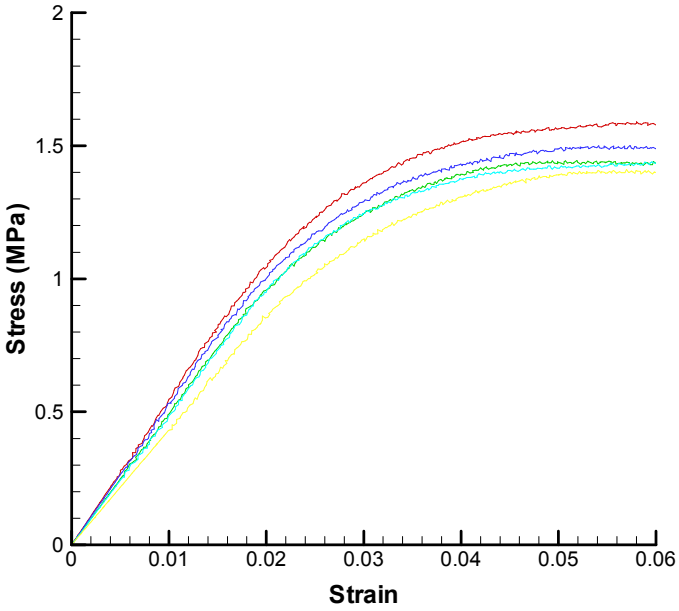

Figure A.6. Quasi-static stress-strain curves of foam at -170 °C with strain rate 0.001 s^{-1}

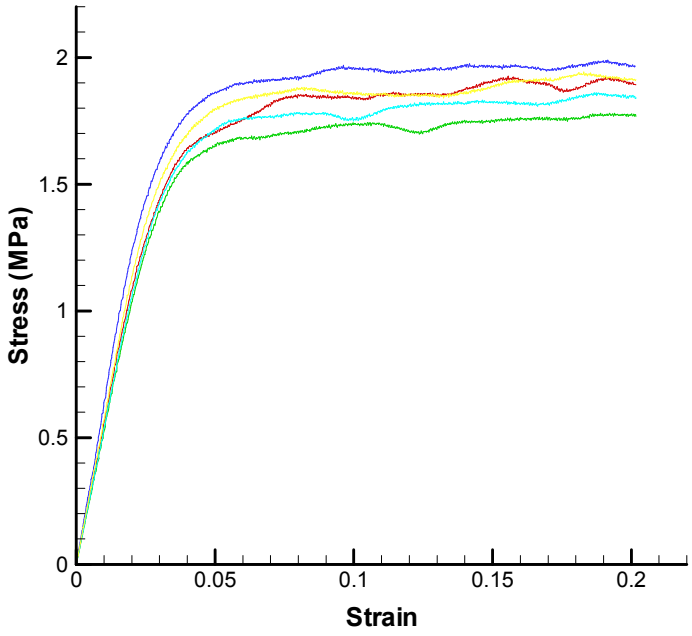

Figure A.7. Quasi-static stress-strain curves of foam at -170 °C with strain rate 0.01 s^{-1}

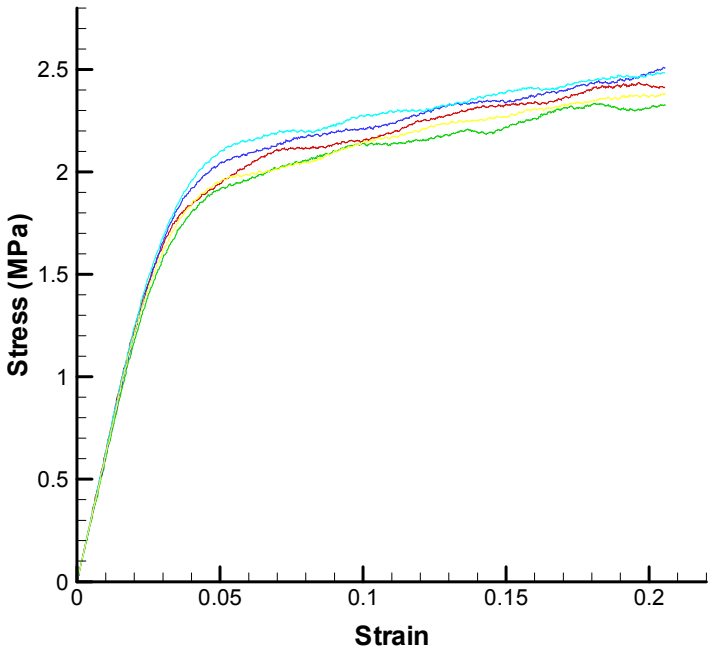

Figure A.8. MTS static stress-strain curves of foam at -170 °C with strain rate 0.1 s^{-1}

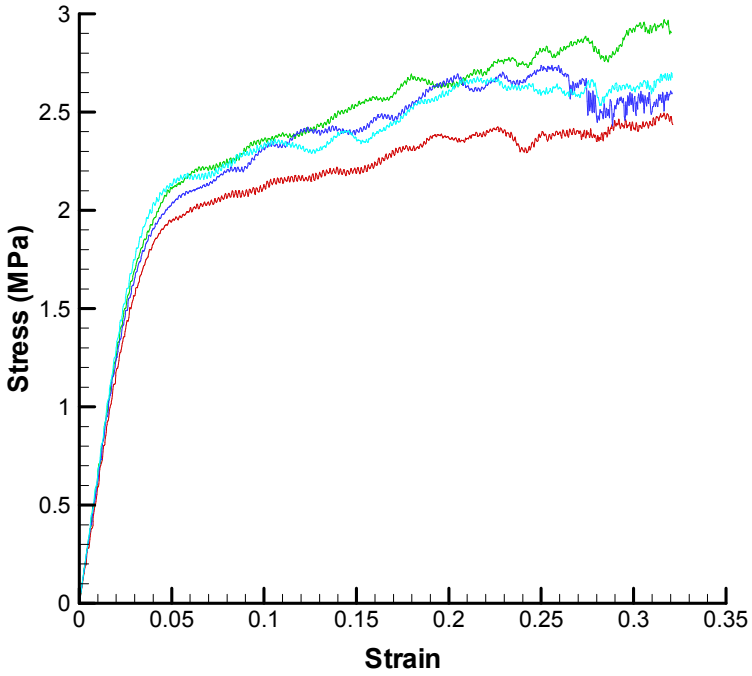

Figure A.9. MTS static stress-strain curves of foam at -170 °C with strain rate 1 s^{-1}

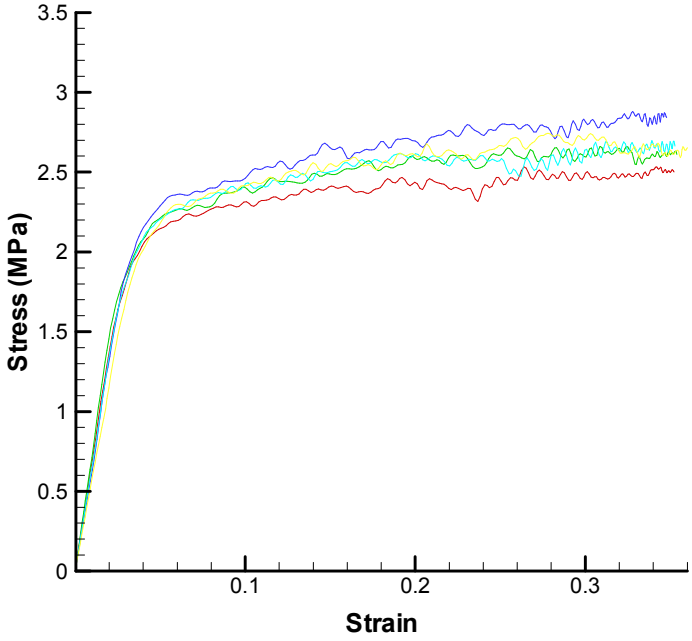

Figure A.10. MTS static stress-strain curves of foam at -170°C with strain rate 10 s^{-1}

VITA

Yanli Zhang

Candidate for the Degree of

Master of Science

Thesis: CHARACTERIZATION OF COMPRESSIVE AND FRACTURE BEHAVIOR, AS WELL AS RESIDUAL TENSILE STRENGTH OF A POLYURETHANE FOAM

Major Field: Mechanical Engineering

Biographical:

Personal Data: Born in Hengshui, China on Nov. 08, 1973, daughter of Wenlu Zhang and Shubiao Gao

Education: Received Bachelor of Science degree in Mechanical Engineering Technology from Oklahoma State University in December, 2004. Will complete the requirements for Master of Science degree in Mechanical Engineering at Oklahoma State University May, 2007.

Experience: Research Assistant**,** 01/2006-present, Polymer Mechanics Laboratory, Oklahoma State University

Engineer, 11/1997-01/1999,Chenchang Building Material Company, Beijing, China.

Product Development Engineer, 07/1994-11/1997
Nankou Building Material Company, Beijing, China

Name: Yanli Zhang Date of Degree: May, 2007

Institution: Oklahoma State University Location: Stillwater, Oklahoma

Title of Study: CHARACTERIZATION OF THE COMPRESSIVE AND FRACTURE BEHAVIORS, AS WELL AS THE RESIDUAL TENSILE STRENGTH OF A POLYURETHANE FOAM

Pages in Study: 52 Candidate for the Degree of Master of Science

Major Field: Mechanical Engineering

Scope and Method of Study: Experiments were conducted on polyurethane foam to determine its compressive strength/modulus, relaxation behavior, fracture toughness, as well as residual tensile strength after repetitive compression at room temperatures and −170 °C.

Findings and Conclusions: Results indicate that, in general, both the Young's modulus and collapse strength increase with the increase of the strain rate at both room temperature and -170 °C. The relationship between Young's modulus and strain rate, between collapse strength and strain rate were fitted into equations. A Prony series was constructed for the average modulus at different strain rates. Young's relaxation master curve was constructed based on time-temperature superposition principle to show property change as a function of time. The critical stress intensity factor and critical energy release rates are determined to be 110.25 $KPa.m^{1/2}$ and 22.25 J/m^2, respectively, from testing of three-point bending specimens with a crack parallel to the fiber plane. Residual tensile strength has been determined to reduce by 40% after 100 cycles of compression at the amplitude about 55% of the collapse compressive strength.

ADVISER'S APPROVAL: Dr. Hongbing Lu